*Conference on Modelling Fluid Flow (CMFF'25)*
*The 19th International Conference on Fluid Flow Technologies*
*Budapest, Hungary, August 26 - August 29, 2025*

# NUMERICAL ANALYSIS OF THE DECELERATED SWIRLING FLOW REGIMES OBTAINED BY USING A MAGNETORHEOLOGICAL CONTROL DEVICE

Raul Alexandru SZAKAL[1], Alin Ilie BOSIOC[2], Sebastian MUNTEAN[1]

[1] Corresponding Author. 2Center for Advanced Research in Engineering Sciences, Romanian Academy- Timisoara Branch, Bv. Mihai Viteazu, No. 24, 300222, Romania. E-mail: raul.szakal@student.upt.ro
[2] University Politehnica Timisoara, Mechanical Engineering Faculty, Bv. Mihai Viteazu, No. 1, 300222, Romania, E-mail: alin.bosioc@upt.ro

## ABSTRACT

The paper focuses on 3D numerical simulations of the decelerated swirling flow conditions in a swirling flow generator. The swirling flow regimes from 1020 *rpm* runaway speed to 870 *rpm* are obtained using a magnetorheological (MR) device at a constant discharge of 30 *l/s*. An 2D Lasser Doppler Velocimetry (LDV) measuring system has been used to measure the mean meridional and tangential velocity profiles in the divergent part of the test section. The 3D numerical simulations have been performed in agreement with real operation conditions. A mixing plane method has been used to transfer the flow between the 3D simplified domains of the swirling flow generator and full 3D test section. The turbulence model *k- ω* and structured mesh type were used for computing the flow in the leaned strouts, stator and rotor's domain. RSM turbulence model has been selected for computing the unsteady flow field in the test section at regimes corresponding to rotor's speed from 990 *rpm* to 870 *rpm*. A time step of $10^{-4}$ *seconds* has been considered for the numerical simulations in the test section. The numerical results against experimental data shows that the employed methodology leads to good results.

**Keywords: decelerated swirling flow, 3D numerical simulation, vortex rope, 2D LDV flow field validation**

## NOMENCLATURE

| | | |
|---|---|---|
| $k$ | [$m^2/s^2$] | turbulence kinetic energy |
| $\varepsilon$ | [$m^2/s^3$] | turbulence dissipation |
| $\omega$ | [1/s] | specific turbulence dissipation |
| $l$ | [-] | dimensionless axis length |
| $Rref$ | [m] | reference throat radius |
| $v$ | [-] | dimensionless velocity |
| $Va$ | [m/s] | axial dimensionless velocity |
| $Vu$ | [m/s] | tangential dimensionless velocity |
| $Vr$ | [m/s] | dimensionless velocity |
| $u_{RMS}$ | [-] | dimensionless root mean square |
| $Q_{op}$ | [l/s] | operation discharge |
| $Vref$ | [m/s] | reference throat velocity |

## 1. INTRODUCTION

Decelerated swirling flow is a particular type of flow common to various hydraulic machinery and combustion applications. The same for the cases of hydraulic turbines with fixed blades as Francis or propeller. While operated at partial discharges for power regulation of the electrical grid the decelerated swirling flow at the conical diffusers of Francis turbines leading to strong pressure pulsations and associated vibrations that hinder the good operation [1]. Moreover, start-stop cycles associated with nowadays operation requirements leads to stress loads on mechanical components and eventually failure of them [2-3]. To better understand the flow behaviour in such operating conditions and to address them with proper flow control methods both experimental and numerical work has been done in the last years [4-6]. Moreover, proper flow control methods should be address to particular flow configurations for better results [7].

The paper aims to investigate via both numerical and experimental procedures the decelerated swirling flow from the swirling flow generator from University Politehnica Timisoara [8]. This device is a surrogate of Francis FLINDT hydraulic turbine and mimics the decelerated swirling flow from the draft tube cone. A magnetorheological (MR) device has been utilized to modify the swirling flow conditions. The swirling flow generator together with experimental and numerical setup are presented in section 2. Section 3 presents the flow field validation

and numerical results. The summarize and conclusions of the performed both numerical and experimental work are presented in the last part of the paper together with future research.

## 2. SWIRLING FLOW GENERATOR. EXPERIMENTAL AND NUMERICAL SETUP

### 2.1. Experimental setup

To examine the swirling flow phenomena and quantify their effects, the swirling flow generator from University Politehnica Timisoara has been used. The test rig was designed to mimics the swirling flow conditions from Francis Flindt hydraulic turbine. As depicted in Figure 1, the test section installed on the test rig is assembled by a swirl generator [8] and a convergent divergent plexiglass test section [9]. The swirl generator consists of two rows of blades placed coaxially on a hub fixed by a nozzle. The stationary first row of blades generates an excess of tangential momentum as a 30 *l/s* discharge passes through the hydraulic passage. The flux of moment of momentum is then redistributed by the second row of blades called rotor. The rotor was designed with 10 blades and acts like a turbine near to the hub and as a pump near to the shroud. In this way, the total pressure of the main flow is increased at the shroud and decreased in the centre area. The conical shape of the nozzle together with the upper part of the test section assembly a convergent duct which diminishes the drag from the rotor's outlet. In this way, a clean swirling flow is generated at the inlet of the cone of the test section. A magneto-rheological brake was embedded in the rotor`s hub to modify the swirl at the inlet of the convergent-divergent test section [10]. Breaking the rotor speed of the rotor leads to different swirling flow configurations. Both mean velocity profile and unsteady pressure can be measured downstream to the magnetorheological controlled rotor by using a Dantek 2D LDV system and unsteady pressure sensors. The major advantage of using an LDV system for flow characterization consists of the non-invasive measuring technique. The 2D LDV measuring system consists of a measuring probe and a 3D traverse system. This setup ensures a displacement of the probe with a step of 0.2 *mm* step along all coordinates (e.g., x, y, z). The W0, W1 and W2 measuring windows allows to measure the mean velocity profiles on both convergent and divergent part of the test section. The associated axis of each measuring window is placed perpendicular to the wall of the test section. The test section has a throat diameter of 0.1 *m* and the cone half-angle is 8.5° on a height of 0.2 *m*. The downstream pipe connected to the outlet of the divergent part of the test section has a diameter of 0.16 *m* and a length of ≈2m.

### 2.2. Numerical setup and operating regimes

A 3D numerical simulation was performed using commercial software Ansys Fluent 6.3[11]. For all numerical investigated flow conditions, a constant discharge of 30 l/s was imposed in agreement with experimental setup. The full 3D unsteady computations for the swirl generator apparatus may not be a very cost-effective method due to the substantial computational resources required. Hence, some simplifications were considered. Instead of considering the full 3D domain of the swirling flow apparatus, the leaned strouts, stator and rotor domain were simplified in agreement with both flow and geometrical periodicity. In order to couple the flow between the simplified computational domains of the swirling flow generator, a mixing plane method has been used. According to Figure 2, the simplified leaned strouts domain (90°) has been discretized with 65k cells, the simplified domain of the stator (27.69°) with 132k cells and the rotor`s domain (36°)

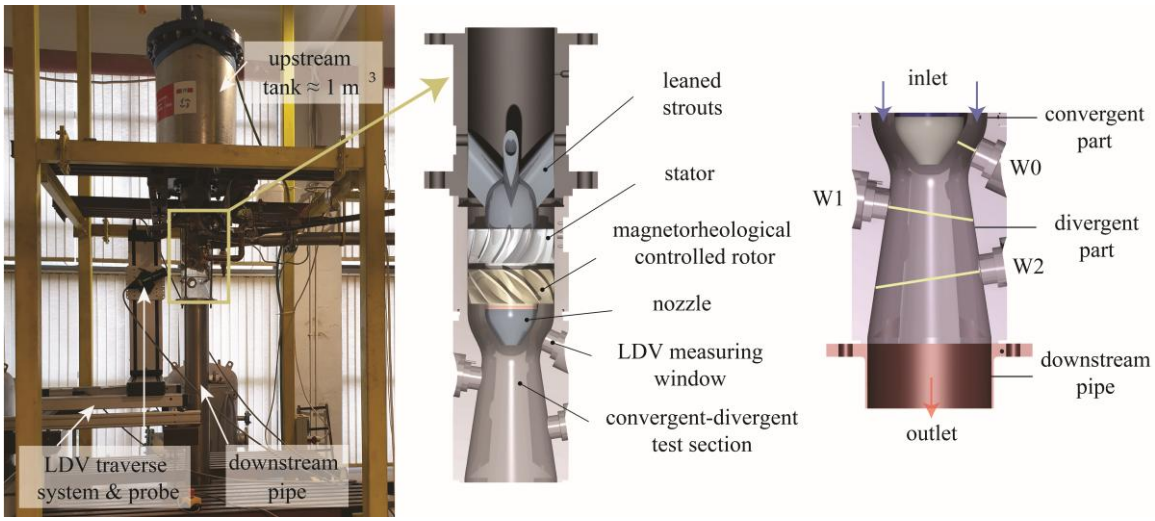


**Figure 1. Test rig for decelerate swirling flow investigation (left), the swirling flow generator (center), detail of the convergent divergent test section (right)**

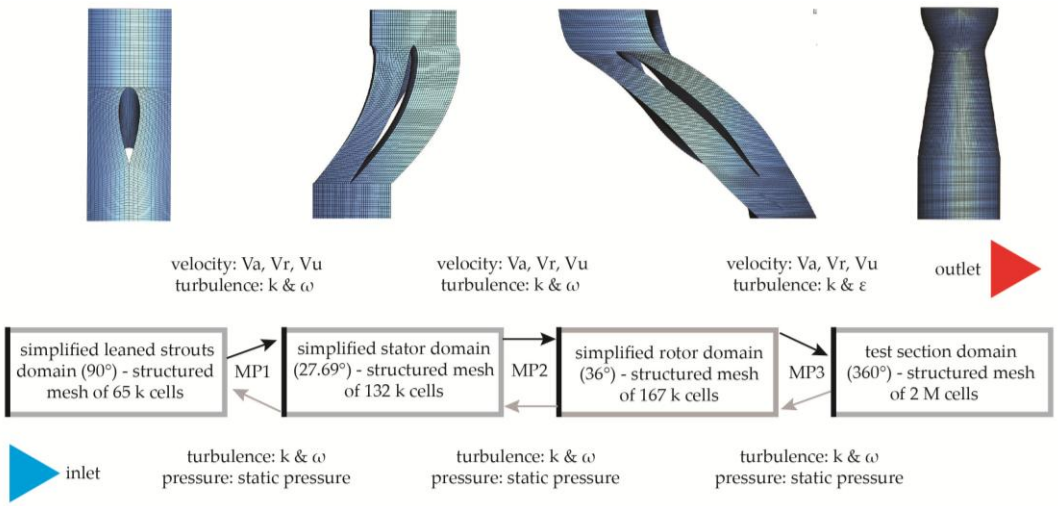


**Figure 2. The computational domain of the swirling flow generator and mixing plane algorithm utilized in numerical simulations**

with 167k cells, respectively. The convergent-divergent test section domain (360°) has been discretized with about 2 million cells. The flow has been transferred in the normal flow direction by imposing at each domain's inlet the following: (i) axial mean velocity (ii) radial mean velocity and (iii) tangential mean velocity profiles together with (iv) turbulence quantities (e.g., $k$, $\omega$ or $\varepsilon$). At the outlet of each domain, the turbulence quantities have been imposed together with the static pressure distribution. Absolute steady state numerical simulations have been performed for the leaned strouts and stator's domain using fast and reliable $k$-$\omega$ turbulence model. For the rotor's domain, a relative steady-state has been considered using same k- ω turbulence model and the angular velocity of it has been imposed in agreement with rotational speed of the rotor from experimental work. The unsteady flow behaviour in the convergent-divergent test section domain with a time step of $10^{-4}$ has been considered together with RSM turbulence model, which has already proven capabilities within such flow configurations [12]. A SIMPLE pressure-velocity coupling method and second order discretization scheme for the equation system have been used. For the flow computations in strouts, stator and rotor's domain the absolute convergence criterion were set to 1e-9 to ensure an accurate enough result. Due to lack of experimental data at the outlet of the test section a radial equilibrium boundary condition has been imposed together with hydraulic diameter of 0.16 and 3% turbulence intensity. RSM model involve dissipation rate term ε which has been obtain from specific dissipation rate $\omega$ by using the following equation:

$$\omega = \frac{\varepsilon}{kC_\mu} \tag{1}$$

where $k$ is the turbulent kinetic energy and $C_\mu$ an emphiric constant (0.09).

## 3. FLOW FIELD VALIDATION AND NUMERICAL RESULTS

Global parameters as volumetric flow rate and flux of moment of momentum are critical parameters to be conserved along each domain considered for the numerical simulations performed. They have been monitored at each mixing plane to ensure that the operating regime has been conserved and ultimately, the computed flow in the convergent divergent test section is closer to the real one. According to our previous work, a maximum relative deviation of 0.3% and 3.5% has been obtained for volumetric flow rate and flux of moment of momentum, respectively along the mixing planes [13]. These results underlined a good transfer of the flow along the mixing planes.

Since our previous work underlined that the computational efforts describe well the flow on the convergent part of the test section (mean velocity profile validation on measuring window W0 at 920 and 870 *rpm*) those results can be found in [14] together with pressure pulsation validation. Hence, the paper extends and discuss the results and validation of the velocity profiles on W1 and W2 measuring windows. W1 and W2 measuring windows are placed in the divergent part of the test section where decelerated swirling flow occurs. Due to the strong adverse pressure gradient and the conical shape, close to the axis a quasi-stagnant region is developed in agreement with both experimental and theoretical studies [15-16]. The mean velocity profile for meridian and tangential velocity has been extracted from the performed numerical simulation. Around 40 time-steps were considered to average the velocity components and obtain the velocity profiles. Both experimental and numerical data were represented in dimensionless form and the following formulas has been used to express the length of the measuring axis $l$ (e.g.,

associated length of W1, W2 measuring windows) and velocity:

$$l = \frac{x}{R_{ref}} \quad (2)$$

$$v = \frac{V}{V_{ref}} \quad (3)$$

$$V_{ref} = \frac{Q_{op}}{\pi \cdot R_{ref}^2} \quad (4)$$

$l$ represents the dimensionless axis length, and it has been obtained by the ratio between $x$ – x coordinate on the $R_{ref}$ – the throat radius ($0.05m$). $v$ represents the dimensionless velocity, and it has been obtained by the ratio between the measured and calculated velocity $V$ to the refence velocity $V_{ref}$ corresponding to the throat velocity. Eq. (4) has been used to obtain the $V_{ref}$, by the ratio of the operating flow rate ($Q_{op}$-$30l/s$) to the throat area. The dimensionless root mean square $uRMS$ of each measuring points has been plotted in vertical bars to express the velocity fluctuation. The dimensionless form has been obtained using the following formula:

$$u_{RMS} = \frac{\sqrt{\sum_{i=o}^{N-1} \frac{1}{N} (u_i - \bar{u})^2}}{Vref} \quad (5)$$

where $N$ is the number of measured points, $u_i$ the instantaneous measured velocity and $\bar{u}$ the average value of the measured velocity.

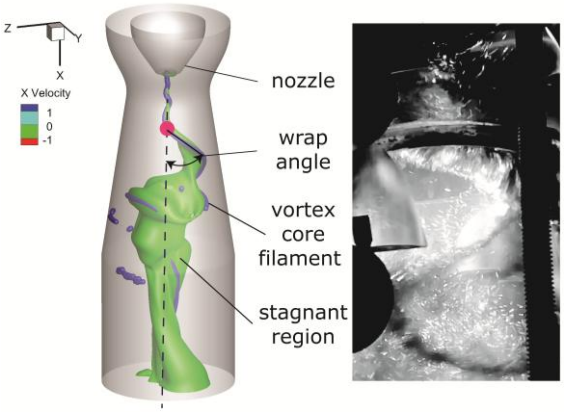


**Figure 3. Vortex rope sketch and experimental visualization**

The structure of the decelerated swirling flow into the draft tube cone is presented in Fig. 3. A vortex rope sketch together with experimental visualization underline the presence of the vortex rope phenomena. The vortex core filament has a spiral-like shape and wraps around a quasi-stagnant region (mean meridian velocity component is negligible). The wrap angle of the vortex core and associated filament is modified by the hydrodynamic regime (e.g. modifying the rotors speed with the magnetorheological device).

The mean velocity field validation for W1 measuring window is presented in Figures 4-6 for the four analysed operating regimes corresponding to rotors speed of 870, 960 and 990 *rpm*, in agreement with speeds obtained using magnetorheological breaking.

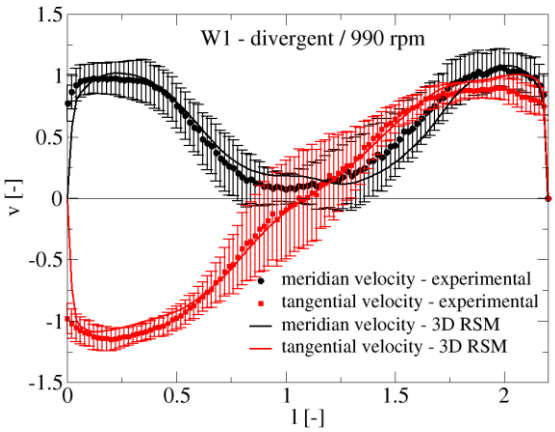


**Figure 4. Mean velocity field – meridian and tangential numerical velocity profiles against experimental data on W1 at 990 *rpm***

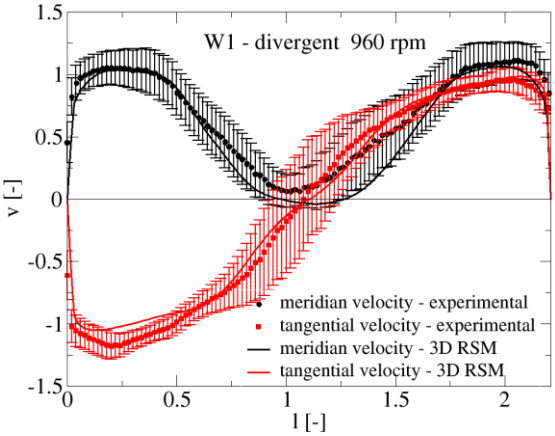


**Figure 5. Mean velocity field – meridian and tangential numerical velocity profiles against experimental data on W1 at 960 *rpm***

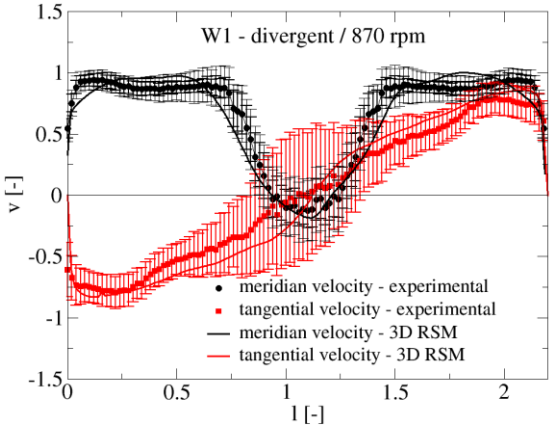


**Figure 6. Mean velocity field – meridian and tangential numerical velocity profiles against experimental data on W1 at 870 *rpm***

The breaking down the rotor's speed using the magnetorheological device from 1020 *rpm* to 870 *rpm* leads to decreasing the flux of moment of momentum at the inlet of the test section [17]. This fact is supported by the results obtained both from 3D numerical simulations using RSM model and 2D LDV mean velocity field on measuring window W1. At 990 *rpm*, the decelerated swirling flow conditions leads to a meridian velocity deficit (values close to 0) of almost 0.3/*l* close to the axis. The maximum dimensionless value of the meridian velocity component is around 1 and it's located at the extremities, close to the wall of the test section. A linear distribution of meridian velocity component was observed within 15% of the axis length (*l*) close to the wall at 990 *rpm*. While slowing down the rotor to 870 *rpm*, the meridian velocity deficit is diminished at around 0.1/*l* in the central area of the test section. However, the linear distribution evidenced at larger rotational speeds increase up to 35% of *l* at 870 *rpm*.

Moreover, while the meridian velocity field tends to become uniform, the central deficit area becomes a recirculation region with negative values for the mean meridian velocities. This behaviour is a consequence of the strong tangential velocity component together with strong adverse pressure gradient which tends to push the main flow close to the wall of the test section. The maximum tangential dimensionless velocity is around 1.2 close to the wall at 990 *rpm* and decrease up to 0.8 at the same area at 870 *rpm*.

Figures 7-9 provides the results obtained from numerical simulation vs. 2D LDV experimental data on W2 measuring window placed in the second part of the divergent area of the test section. At large rotor's speed (e.g., 990-960 *rpm*), the strong swirling flow conditions support the formation of the central quasi stagnant region close to the axis of the test section. The quasi-stagnant region (with meridian velocities oscillates around 0 value) covers up to 40-45% of *l* at 990 and 960 *rpm*, respectively. In the performed 3D numerical simulations, the quasi-stagnant region identified on W2 at large rotor's speeds in meridian velocity component is overestimated due to the lack of backflow pressure conditions and the radial equilibrium condition imposed at the outlet. As opposed to the W1, on W2 measuring window the meridian velocity distribution is not linear close to the wall and has a peak-like distribution due to larger area of the test section at that region. However, while the rotor's speed decreased to 870 *rpm*, the meridian velocity component distribution tends to achieve the linear distribution but just on around 5-10% of *l* closed to the wall. If al large rotos speed of 990-960 *rpm*, the tangential velocity distribution has a central solid-rigid behaviour close to the axis, at 870 *rpm*, a flatten region of tangential velocity has been identified. The results at 870 *rpm* show more scattering in the experimental data, which appears to be due to the magnetorheological device s failure keep the rotor speed constant. This happened due to washing out effect of magnetorheological fluid evidenced in our previous work [10].

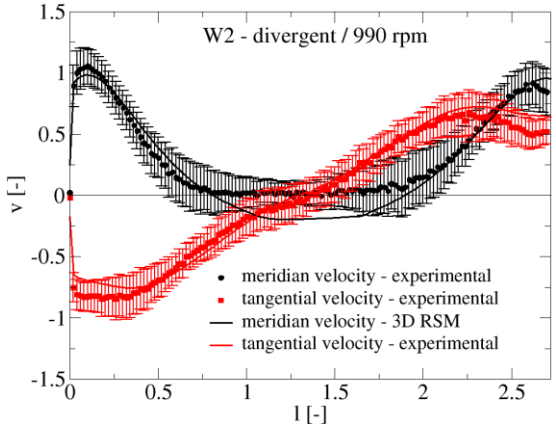


**Figure 7. Mean velocity field – meridian and tangential numerical velocity profiles against experimental data on W2 at 870 *rpm***

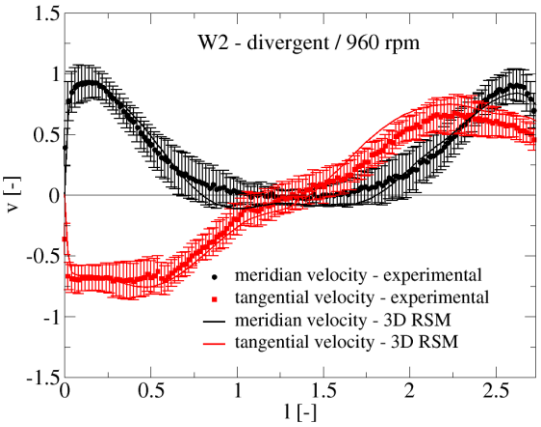


**Figure 8. Mean velocity field – meridian and tangential numerical velocity profiles against experimental data on W2 at 920 *rpm***

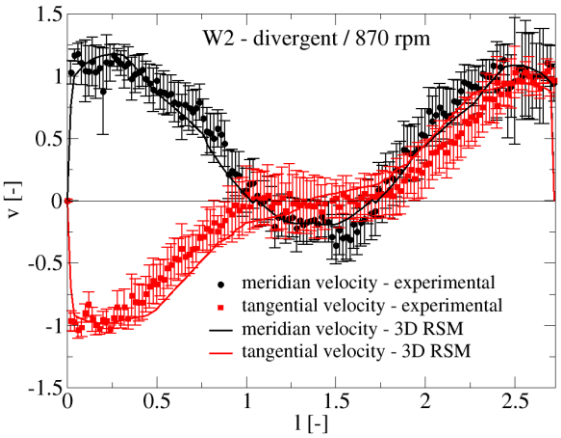


**Figure 9. Mean velocity field – meridian and tangential numerical velocity profiles against experimental data on W2 at 990 *rpm***

Using the RSM turbulence model to compute the flow in the swirling flow generator is a good cost-

effective choice due to the results obtained at analysed operating points. The 3D numerical results describe the mean flow fields in the divergent area of the test section in agreement with experimental data measured with 2D LDV system. Moreover, this good agreement is supported by overlap of the numerical results with experimental ones within the $u_{RMS}$ band presented in vertical bars. The improved flow conditions of the swirl generator obtained with the magnetorheological device validates the 3D numerical simulations.

## 4. CONCLUSIONS

The numerical experiment has been conducted to better understand and validate a reliable working methodology for computing 3D decelerated swirling flow conditions in the swirling flow generator.

The paper presents the numerical and experimental results obtained for different decelerated swirling flow configurations in the swirling flow generator. A 2D LDV measuring system has been used to obtain the mean flow field in the divergent part of the test section on the associated W1 and W2 measuring axis. A magnetorheological brake has been used in experimental work to control the rotor's speed from 1020 to 870 *rpm*. The boundary conditions imposed in the 3D numerical setup were set to fulfil the real operating conditions. The overall setup and particular RSM turbulence model together with imposed boundary conditions showing good agreement with experimental data.

The study stands for a good validation of the mean velocity flow field in the swirling flow generator and together with unsteady pressure field validation would ensure a proper understanding of flow behaviour. The analysis of the mean velocity flow field shows that the flow can be improved overall if the flux of moment of momentum decreases, and the central stagnant region is filled.

Hence, a control method to address these particular types of flow should ensure a filling the meridian velocity deficit identified in the central area and diminishing the excess of high tangential velocity component close to the wall of the cone in hydraulic turbines. Building upon the validated numerical analysis, future work will be done to extend the understanding of vortex rope evolutions at different decelerated swirling flow configurations. The evolution of the associated filament of the vortex rope together with both unsteady pressure and mean velocity flow filed validation will be further done.

## ACKNOWLEDGEMENTS

The work of the first author was supported both by the RA-TB/CFATR/LHC multiannual research program 2021–2025 and by a grant of the Ministry of Research, Innovation and Digitization, CCCDI UEFISCDI, project number PN-IV-P7-7.1-PED-2024-1113, within PNCDI IV.

## REFERENCES

[1] Kougias. I., et al., 2019, "Analysis of emerging technologies in the hydropower sector", *Renewable and Sustainable Energy Reviews,* Vol. 113, pp. 109257.

[2] Frunzăverde. D., *et al.*, 2010, "Failure analysis of a Francis turbine runner", *IOP Conference Series: Earth and Environmental Science,* Vol. 12, pp. 012115.

[3] Luna-Ramírez. A., Campos-Amezcua, A., Dorantes-Gómez, O. Mazur-Czerwiec, Z. and R. Muñoz-Quezada, 2016, "Failure analysis of runner blades in a Francis hydraulic turbine — Case study", *Engineering Failure Analysis,* Vol. 59, pp. 314-325.

[4] Ciocan, G., Iliescu, M., Vu, T.C., Nennemann, B. and Avellan, F., 2007, "Experimental Study and Numerical Simulation of the FLINDT Draft Tube Rotating Vortex", *Journal of Fluids Engineering,* Vol. 129, pp. 146-158.

[5] Javadi, A., Bosioc, A., Nilsson, H., Muntean, S. and Susan-Resiga, R., 2016, "Experimental and Numerical Investigation of the Precessing Helical Vortex in a Conical Diffuser, With Rotor-Stator Interaction", *Journal of Fluids Engineering-Transactions of the Asme*, Vol. 138(8), pp. 081106.

[6] Bosioc, A.I., and Tanasa, C., 2020, "Experimental study of swirling flow from conical diffusers using the water jet control method", *Renewable Energy*, vol. 152, pp. 385-398.

[7] Skripkin, S. and Shtork, S., 2025, "Active vortex control downstream the turbine runner in the Francis hydro turbine model", *Thermophysics and Aeromechanics*. Vol. 31, pp. 819-830.

[8] Susan-Resiga, R., Muntean, S., Tanasa, C. and Bosioc, A.I., 2008. Hydrodynamic Design and Analysis of a Swirling Flow Generator, in Proc. *4th German-Romanian Workshop on Turbomachinery Hydrodynamics* (Stuttgart, Germany)

[9] Bosioc A, Susan-Resiga R and Muntean S 2008 Design and manufacturing of a convergent-divergent test section for swirling flow apparatus, in Proc. *4th German-Romanian Workshop on Turbomachinery Hydrodynamics* (Stuttgart, Germany)

[10] Szakal, R., Bosioc, A.I., Muntean, S., Susan-Resiga, D. and Vekas, L., 2019, "Experimental Investigation of a Magento-Rheological Brake Embedded in a Swirl Generator Apparatus", *Materials Design and Application II Advanced Structured Materials,* Vol. 98, pp. 265-279.

[11] Fluent Inc 2001 Fluent 6. User Guide

[12]Muntean, S., Tanasa, C., Bosioc, A.I. and Mos, D.C., 2016. "Investigation of the Plunging Pressure Pulsation in a Swirling Flow with Precessing Vortex Rope", *IOP Conf. Ser.: Earth Environ. Sci.* Vol. 49, pp. 082010.

[13]Muntean, S., Susan-Resiga, R. F. and I. Anton, 2004, "Mixing interface algorithm for 3D turbulent flow analysis of the GAMM Francis turbine", *Modelling Fluid Flow*, pp. 359-372.

[14]Szakal, R. A., Muntean, S., Bosioc, A. I., Susan-Resiga, R. and Vékás, L., 2021, "3D numerical investigations of the swirling flow in a straight diffuser for the variable speed values of the rotor obtained with a magneto-rheological brake," in *IOP Conference Series: Earth and Environmental Science*, Vol. 774, pp. 012019.

[15]Nishi, M., Matsunaga, S., Okamoto, S,. Uno, M., and Nishitani, K., 1988, "Measurement of Three-dimensional Periodic Flow in a Conical Draft Tube at Surging Condition," *Flow in Non-Rotating Turbomachinery Components*, Vol. 69, pp. 173-184.

[16]Keller, J. J., Egli, W., and Althaus, R., 1988, "Vortex Breakdown as a Fundamental Element of Vortex Dynamics," *Journal of Applied Mathematics and Physics*, Vol. 39, pp. 404-440.

[17]Muntean, S., Bosioc, A.I., Szakal, R.A., Vékás, L., and Susan-Resiga, R.F., 2017, "Hydrodynamic Investigations in a Swirl Generator Using a Magneto-Rheological Brake," in *Materials Design and Applications*, L. F. M. d. Silva, Ed. Cham: Springer International Publishing, Vol. 65, pp. 209-218.